JVST A
Journal of Vacuum Science & Technology A

ARTICLE

pubs.aip.org/avs/jva

Use of an auxiliary electrode to control plasma properties at the wafer edge in inductively coupled plasmas with a substrate bias

Cite as: J. Vac. Sci. Technol. A 43, 063001 (2025); doi: 10.1116/6.0004847
Submitted: 15 July 2025 · Accepted: 11 September 2025 ·
Published Online: 26 September 2025

Tugba Piskin,[1,a] Saravanapriyan Sriraman,[2,b] Hyunjae Lee,[3,c] Sang Ki Nam,[3,d] and Mark J. Kushner[1,e]

AFFILIATIONS

[1]Electrical Engineering and Computer Science Department, University of Michigan, Ann Arbor, Michigan 48109-2122
[2]Lam Research Corporation, 4400 Cushing Parkway, Fremont, California 94538
[3]Mechatronics Research, Samsung Electronics Co., Ltd., 1-1 Samsungjeonja-ro, Hwaseong-si, Gyeonggi-do 18448, South Korea

Note: This paper is part of the Special Topic Collection: Papers from the AVS 70th International Symposium.
[a]**Present address:** Lam Research Corporation, 11361 SW Leveton Drive, Tualatin, Oregon 97062;
electronic mail: Tugba.Piskin@lamresearch.com
[b]**Electronic mail:** Saravanapriyan.Sriraman@lamresearch.com
[c]**Electronic mail:** hj0928.lee@samsung.com
[d]**Electronic mail:** sangki.j.nam@samsung.com
[e]**Author to whom correspondence should be addressed:** mjkush@umich.edu

ABSTRACT

In plasma etching of microelectronics devices, a continuing challenge is maintaining uniform fluxes of radicals and ions, and ion energy and angular distributions (IEADs) to the edge of the wafer. In plasma etching of high aspect ratio features requiring ion energies of several keV, ions incident onto the wafer should have trajectories that are normal to the wafer. At the edge of the wafer, the transition between the wafer and structures surrounding the wafer (often called the focus ring) produce curvature to the sheath responsible for accelerating ions into the wafer. The result is an angular tilt away from the normal of incident ions onto the edge of the wafer. In this paper, we discuss results from a computational investigation of using an auxiliary electrode (E2) surrounding the primary bias electrode (E1) to control sheath curvature at the edge of the wafer. The test system is an inductively coupled plasma sustained in an Ar/O_2 mixture with a 5 MHz bias applied to the substrate E1. We found that with optimum placement of and voltage applied to the auxiliary electrode E2, IEADs incident onto the wafer could be made uniform to the edge of the wafer. The use of the auxiliary electrode E2 does affect the characteristics of E1, for example, modulating the DC bias and power deposition; however, these effects are small. The use of E2 does bring additional complexities and costs, which should be considered in optimizing the system.

I. INTRODUCTION

A continuing challenge in plasma processing for semiconductor fabrication is utilizing the full diameter of the wafer to produce high quality devices.[1–3] In order to achieve this goal, the flux of plasma produced radicals and ions, and the energy and angular distribution of ions (IEADs), should be uniform across the wafer.[4] For high aspect ratio (HAR) plasma etching,[5] typical metrics are better than 1% uniformity in fluxes across the wafer and ion angular distributions to within 1° of the normal for ions having energies of up to several keV.[6,7] Due to the discontinuity in material properties transitioning from the wafer to the structures surrounding the substrate (typically called the focus ring, FR), these metrics are particularly challenging to achieve within several mm of the edge of the wafer.[1,8–10] The challenge in producing optimal devices in this region is often referred to as *edge exclusion*.[1]

One of the major causes of edge exclusion is the tilt of the ion angular distribution (IAD) away from the normal onto the edge of

the wafer.[4] This tilt in large part originates from curvature in the plasma sheath bounding the wafer at its edge.[11] The electric field that accelerates ions into the wafer is usually oriented perpendicular to the contour of the sheath. A sheath that is parallel to the wafer will, in the absence of collisions, accelerate ions into the wafer normal to the surface. A sheath that has curvature will initially accelerate ions into the wafer with a non-normal trajectory. The angle of incidence of an ion onto the wafer is also influenced by the trajectory of the ion entering the sheath.[12] Even for a sheath parallel to the wafer, an ion entering the sheath with a significant velocity component parallel to the wafer will arrive at the wafer with a non-normal trajectory.[13]

Several remedies have been investigated and implemented to reduce edge exclusion resulting from non-normal (or tilted) ion trajectories due to sheath curvature at the transition between the wafer and FR. These remedies include managing the material properties of the FR to align with those of the wafer,[14] extending the biased electrode beyond the edge of the wafer,[15] adjusting the height of the FR[16,17] and managing the capacitance and resistivity of the FR to minimize the impedance variation.[15,18] Although these remedies meet the goal of controlling sheath curvature, they are also static solutions. With static solutions, these remedies are difficult to change during a given recipe where, for example, power deposition or a gas mixture may change, which, in turn, might change sheath properties. A remedy that can be adjusted in real time and so respond to changes in the recipe would provide additional opportunities to tune a process to address edge exclusion.

An effective, dynamic method for managing the uniformity of fluxes and IEADs to the edge of the wafer is the adjustable focus ring. Using this technique, the height difference between the surfaces of the wafer and the FR can be dynamically changed in response to changes in plasma conditions or erosion of the FR.[19] With this difference in height being one of the most significant parameters producing or remedying sheath curvature at the wafer edge, dynamic control of the FR height is a powerful control technique.[10,20] In addition to the geometrical and physical properties of the focus ring, its electrical and thermal designs also have strong influences on wafer edge characteristics. Managing FR properties include thermal tuning of the FR,[21] coupling the focus ring to the ground with an electrode,[22,23] and embedding an electrode in the FR to control the electric field at the edge of the wafer.[24]

In this paper, we discuss results from a computational investigation of using an auxiliary ring electrode to control sheath curvature at the edge of the wafer and so control ion trajectories onto the wafer in the edge-exclusion zone. The test system is an inductively coupled plasma (ICP) sustained in an Ar/O_2 mixture at 10 mTorr with a capacitively coupled substrate bias. The auxiliary ring electrode is imbedded in the FR and driven by a separate radio frequency (RF) power supply. The intent of the auxiliary ring electrode is to control sheath curvature at the edge of the wafer and enable ion trajectories to be uniformly normal to the edge of the wafer. We found that sheath curvature can be controlled by applying high voltage biases to the auxiliary electrode, which results in straightening otherwise tilted ion trajectories to the edge of the wafer. A potential advantage of this method is that by controlling the voltage and frequency applied to the auxiliary electrode, adjustments to ion trajectories to the edge of the electrode can be made in real time as changes are made in the recipe. This remedy does come at the cost of additional power deposition and circuit complexity, and potentially additional erosion of the FR.

The model used in this investigation is described in Sec. II. Results from a parametric investigation of the use of the auxiliary electrode to adjust ion trajectories onto the wafer are discussed in Sec. III. Our concluding remarks are in Sec. IV.

II. DESCRIPTION OF THE MODEL

The simulation of plasma dynamics was performed using the Hybrid Plasma Equipment Model (HPEM) described in detail in Refs. 25–27. A brief summary is given here. The HPEM is a two-dimensional (2D) hydrodynamics model consisting of modules that address different phenomena while exchanging data with other modules. The main modules used in this work are the Electromagnetics Module (EMM), the Fluid Kinetics-Poisson Module (FKPM), the Electron Energy Transport Module (EETM), and the Plasma Chemistry Monte Carlo Module (PCMCM).

The amplitude and phase of electromagnetic fields produced by the antenna (coils) and absorbed in the plasma are computed in the EMM using a frequency domain solution of the wave equation. The EMM employs a circuit model for a matchbox interfacing the power supply to the antenna, which provides the voltage on the antenna.[28,29] The voltage on the antenna produces electrostatic-capacitive coupling of the antenna to the plasma.

The FKPM integrates continuity, momentum, and energy equations, solving for neutral and charged heavy particle densities, fluxes, and temperatures. Poisson's equation is solved simultaneously with continuity equations for charged particles, which provides surface and volume charge densities, needed to produce the electrostatic potential. The voltage boundary conditions are the time varying potentials applied to electrodes (including the antenna) and zero potential on the grounded chamber, which bounds the computational domain. The electron flux is obtained from a Scharfetter–Gummel drift-diffusion model, also within the FKPM, with the mean electron energy being provided by the solution of the electron energy transport equation. Transport and rate coefficients for bulk electrons are produced from electron energy distributions (EEDs) obtained from solutions of Boltzmann's equation using a stationary two-term spherical harmonic solution.

EEDs for sheath accelerated electrons produced by secondary emission by ions were calculated using a Monte Carlo simulation in the EETM using electrostatic fields produced the FKPM and electromagnetic fields from the EMM. Electron impact rate and transport coefficients were then produced from the EEDs for use in the FKPM. Ion trajectories onto the substrate or other surfaces are tracked in the PCMCM using Monte Carlo methods. The end result is IEADs onto the wafer as a function of position.

Separate DC biases are computed for the primary bias (E1) and auxiliary (E2) electrodes. The DC biases are produced by integrating currents flowing into the blocking capacitors placed between the power supply and electrode. The total current collected by a powered electrode is computed by performing an integral over its surface area of the sum of conduction current density and displacement current density. A similar integral is performed for

current collected by metal surfaces on the grounded side of the circuit. These currents are then used to charge the blocking capacitors. The currents flowing into grounded surfaces are apportioned to the bias and auxiliary blocking capacitors in proportion to the currents flowing into the powered electrodes. If these two currents (grounded surface and powered electrode) flowing into the blocking capacitor averaged over the RF cycle are not equal, then there is a net charge placed on the capacitor and generation of the DC bias, V_{DC}. The charging process and V_{DC} naturally come to a steady state when the currents on the powered and grounded sides of the circuit are equal.

Simulations were performed for ICPs sustained in Ar/O_2 gas mixtures as being representative of a mildly electronegative gas mixture. The reaction mechanism used for Ar/O_2 is the same as in Ref. 30.

The model geometry is shown in Fig. 1. The system is an ICP sustained in a cylindrically symmetric chamber 27 cm in radius with a plasma zone 19 cm tall between the wafer and a 2 cm thick dielectric window. The outer boundary of the computational domain (sidewalls, top and bottom) is a grounded metal. Air occupies the space above the dielectric window.

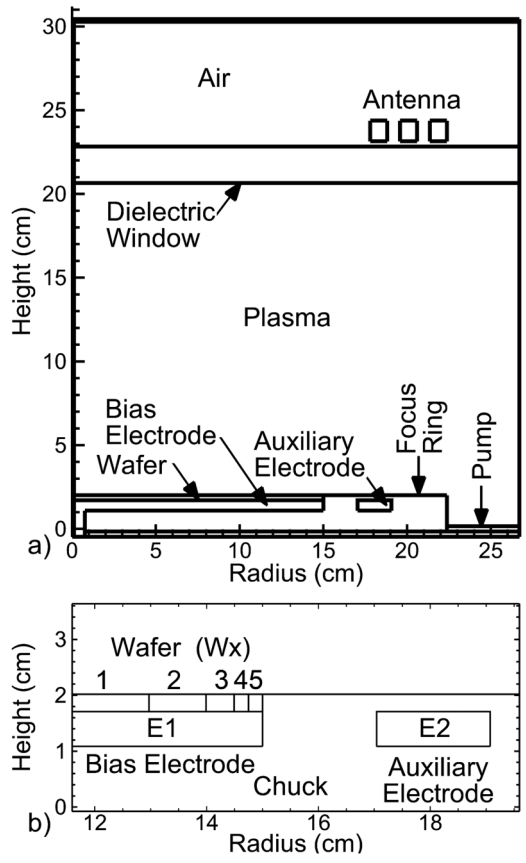

FIG. 1. Geometry for the simulation. (a) The cylindrically symmetric ICP reactor is powered by a three-turn antenna, a primary bias electrode (E1), and an auxiliary electrode (E2). (b) IEADs are collected on five locations (W1–W5) on the wafer, with W5 being at the edge of the wafer.

The plasma is sustained by a three-turn antenna, which is interfaced to a 10 MHz power supply through a match box, which is tuned to minimize reflected power from the antenna. The antenna delivers mixed inductive and capacitive power resulting from the voltage drop across the antenna. Gas is injected uniformly through the dielectric window, approximating a showerhead, and exhausted through the annular pump surrounding the focus ring. Secondary electron emission by ions occurs on all plasma facing surfaces with a probability of 0.01.

The primary bias is applied to electrode E1, 6.2 mm thick, whose diameter matches a 30 cm silicon wafer (relative permittivity $\varepsilon_r = 11.8$ and conductivity $\sigma = 0.05$ S/cm) placed on top of the electrode. The electrode E1 is surrounded by a dielectric FR (relative permittivity $\varepsilon_r = 9.3$ and conductivity $= 10^{-15}$ S/cm). The auxiliary electrode E2, also 6.2 mm thick, is embedded in the FR, offset from electrode E1 by 2 cm. Electrode E2 has a width of 2 cm. DC bias voltages on blocking capacitors between the power supplies and electrodes are separately computed for E1 and E2 as described above. Both electrodes are interface to their power supplies through 100 nF blocking capacitors. The top surface of electrode E2 is 3 mm below the surface of the FR. IEADs (sum of all ions) were collected for ions incident on five regions of the wafer, indicated in Fig. 1(b). W1 provides IEADs averaged over the wafer for a radius less than 13 cm. Regions W2–W5 are centered at radii of 13.5, 14.25, 14.6, and 14.9 cm, with W5 representing the outermost 2 mm of the wafer.

When no voltage is applied to E2, the metal electrode is replaced with a dielectric having a conductivity of 1 S/cm. This conductivity is large enough that there is an insignificant electric field in its interior (essentially constant voltage), and the material appears to be an electrically floating metal. When a voltage is applied to E2, we assume that the material is a perfect metal with a constant voltage throughout its interior. This voltage then becomes a boundary condition in solving Poisson's equation for the electric potential. The conductivity of E2 is then not necessary for the solution.

III. CONSEQUENCES OF THE AUXILIARY ELECTRODE ON IEADs ONTO THE WAFER

The base case operating conditions are an ICP sustained in an $Ar/O_2 = 80/20$ gas mixture at 10 mTorr and a flow rate of 100 sccm. The forward power from the antenna supply is 450 W at 10 MHz. Of that power, 43 W is dissipated resistively by the coil and by capacitive coupling to the plasma, and 407 W is dissipated by inductive coupling to the plasma. The voltage drop across the antenna (6.3 μH inductance) was 910 V. For the base case, which serves as a reference, there is no voltage applied to E2 and there is no connection to ground for E2. The material corresponding to E2 was replaced with a dielectric having a conductivity of 1 S/cm. The bias frequency on the substrate is 5 MHz with an amplitude of 1200 V with a blocking capacitor between the power supply and electrode E1. Although it is more common to hold bias power constant or to control bias power in semiconductor manufacturing, in this investigation, we held bias voltage constant. Operating with

a constant bias voltage enabled better side-by-side comparisons of IEADs when changing the properties of E2.

Plasma properties for the base case are shown in Fig. 2. The inductive power deposition has a maximum of 0.18 W/cm^3 producing a maximum electron density of 4.5×10^{10} cm^{-3}. The DC bias on the blocking capacitor for E1 is −1050 V, which produces a maximum cathodic voltage drop of −2250 V. This voltage drop produces a sheath width of 1.4 cm at the peak of the cathodic portion of the RF cycle. (The peak of the cathodic portion of the RF cycle refers to the instant that the voltage on the electrode is most negative and when typically the sheath at the surface of the wafer is at its maximum extent.) The sheath width is essentially constant for radii <14.3 cm [Figs. 2(b) and 2(c)], producing a sheath boundary parallel to the wafer. Electric field vectors indicating the direction of ion acceleration are perpendicular to the substrate [Fig. 2(c)]. At radii >14.3 cm, the sheath begins to decrease to a width of 2.5 mm at a radius of 16.6 cm over the FR. This transition in sheath width produces curvature to the sheath boundary. The curvature in the sheath edge produces electric field vectors oriented at an inward angle as large as 28°.

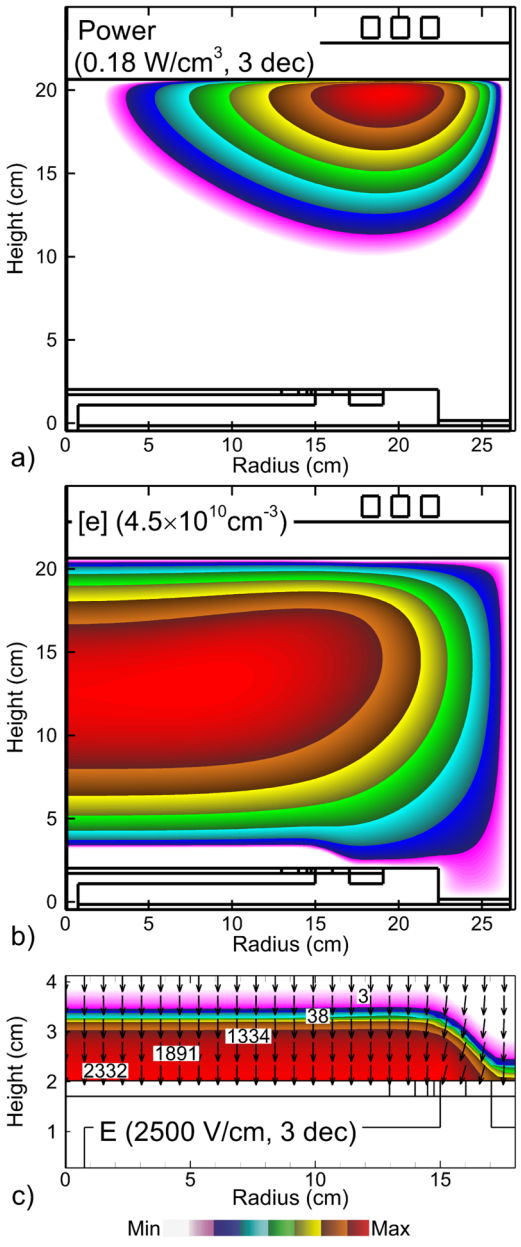

FIG. 2. Plasma properties for the base case (Ar/O_2 = 80/20, 10 mTorr, 450 W, 1200 V bias). (a) Inductive power deposition (log-scale over three decades), (b) electron density at the peak of the cathode cycle when the sheath is at its maximum extent, and (c) an electric field at the peak of the cathodic cycle (log-scale over three decades). The vectors show only the direction of the electric field. Maximum values are indicated in each image.

The thinning of the sheath is a consequence of charging the capacitance of the focus ring.[27] From a circuit perspective, the FR is a dielectric in series with the electrode E1 and the conductive plasma—essentially a capacitor. During the RF cycle, the capacitance of the FR charges and discharges, providing current continuity between the conduction current in the plasma and electrode E1 by passing displacement current through the FR. Following an electric field line originating on E1, passing through the FR and into the plasma, the voltage applied to E1 is sequentially dropped between the capacitance of the FR, the capacitance of the sheath on top of the FR, and the resistance of the bulk plasma. The majority of this voltage is divided between the capacitance of the FR and the capacitance of the sheath. With the capacitance of the FR being smaller than that of the sheath (and having a larger impedance), the FR preferentially charges compared to the sheath. As the capacitance of the FR charges, voltage is removed from the sheath above the FR, which then produces a thinner sheath. The transition from a thick sheath above the wafer to a thin sheath above the FR produces sheath curvature.

The IEADs summed for all ions incident on regions W1–W5 of the wafer are shown in Fig. 3 without voltage on the auxiliary electrode E2. The angle averaged ion energy distributions (IEDs) and energy averaged ion angular distributions (IADs) are in Fig. 4. The energy width of the IEADs is fairly narrow, about 300 eV for a maximum energy of about 1950 eV. This narrow width in energy results from the sheath being in the thick sheath limit. For these conditions, ions require several rf periods to cross the sheath and so arrive at the wafer with an energy corresponding to the average sheath potential.[31,32]

The IEADs have essentially normal angle of incidence onto the wafer for radii <14.3 cm (W2). At larger radii, the curvature in the sheath shown in Figs. 2(b) and 2(c) produces a tilt in angle of the IEAD. Beginning at a radius of 14.5 cm (W3), the tilt increases from a few degrees to as large as 15–20° at the edge of the wafer (W5). The energy widths of the IEADs and IEDs moderately increase with increasing radius. This broadening in energy is a result of the sheath at the edge of the wafer being, on average, thinner than over the center of the wafer. The thinner sheath shortens the transit time of ions across the sheath and enables the ions to better respond to the instantaneous electric fields.[32,33] That said, the effect is not large, a broadening of only 80–90 eV.

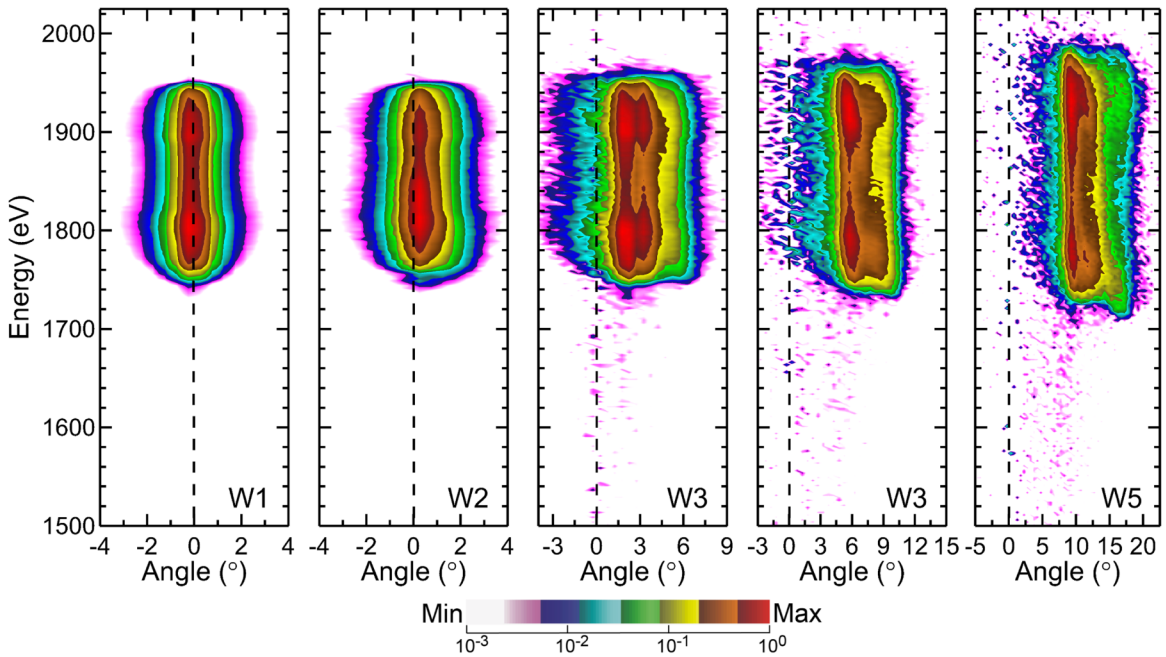

FIG. 3. IEADs incident onto the wafer for the base case without a bias on electrode E2 at positions W1–W5 as noted in Fig. 1(b). Images are plotted on a three-decade log-scale. Note that the range of angles may differ for each location. The dashed line indicates normal incidence. Positive angles are for ions whose trajectories are pointing toward the center of the wafer. Negative angles are for ions with trajectories pointing radially outward.

Applying RF voltage to the auxiliary electrode E2 has the goal of modulating the sheath above the FR and reducing the curvature of the sheath at the edge of the wafer. The curvature of the sheath is largely responsible for the non-normal trajectories of ions incident onto the edge of the wafer. The electron density and direction of the electric field at the peak of the cathodic cycle are shown in Fig. 5 when applying voltage at 5 MHz to auxiliary electrode E2 with an amplitude

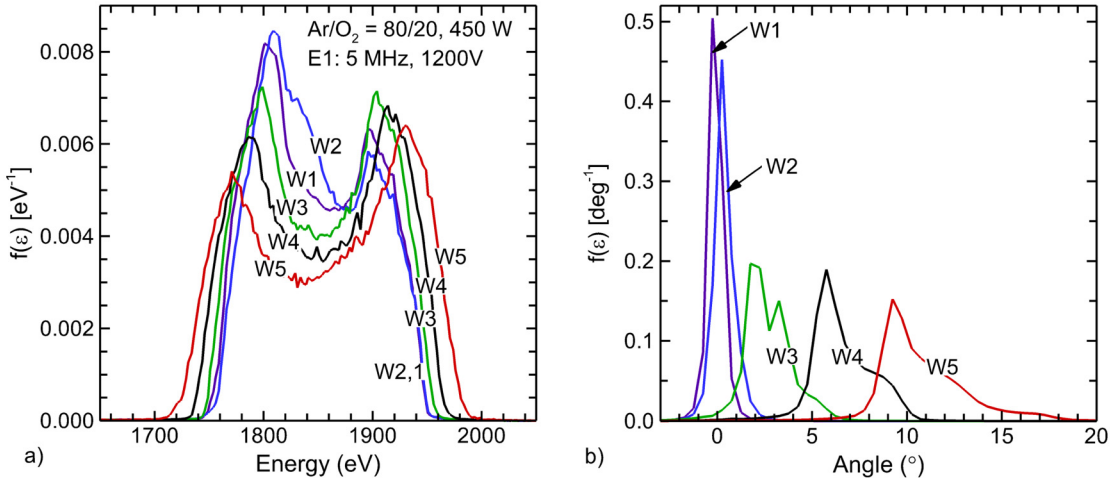

FIG. 4. IEDs and IADs for all ions incident onto the wafer without a bias on electrode E2 at the positions noted in Fig. 1(b). (a) Angular averaged ion energy distribution (IEDs) and (b) energy averaged angular distributions (IADs). Positive angles are for ions whose trajectories are pointing toward the center of the wafer. Negative angles are for ions with trajectories pointing radially outward.

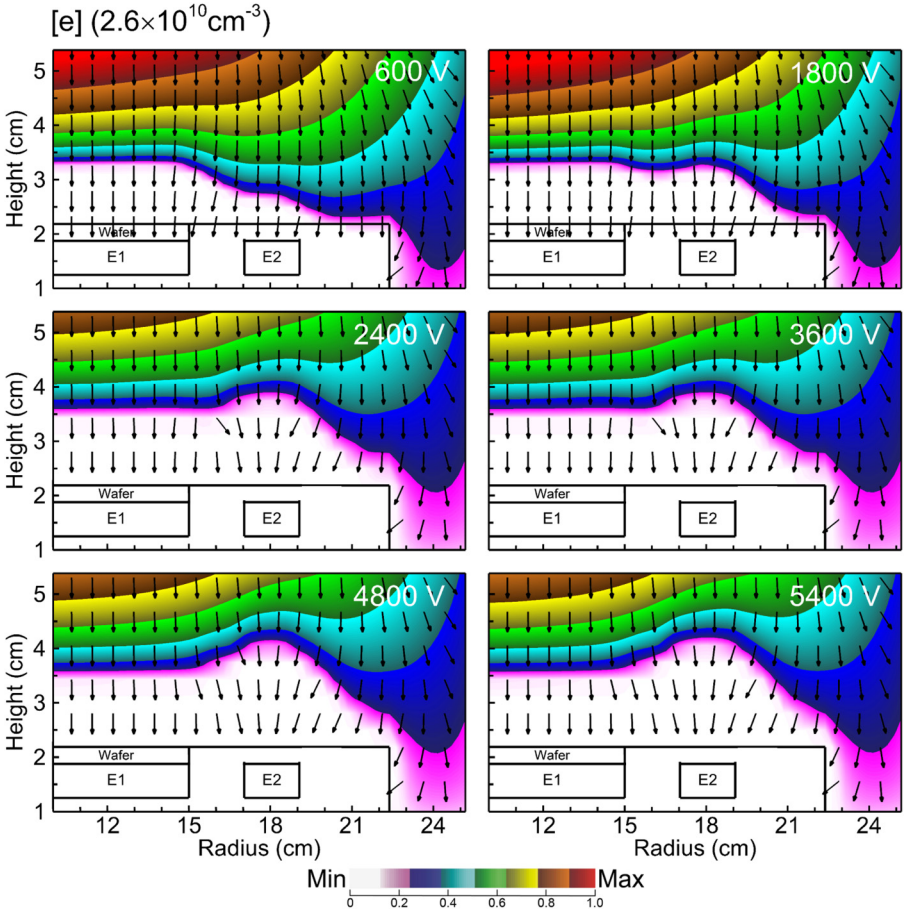

FIG. 5. Electron density and electric field vectors over the wafer edge and the focus ring for voltage at 5 MHz applied to electrode E2 having amplitudes of 600–5400 V. The electron density has a maximum value at the top of the image. Vectors only show direction of the electric field. The vertical scale in the images is expanded by a factor of 2 for clarity.

of 600–5400 V. The RF voltage applied to E1 and to E2 is in phase.

With smaller amplitudes of voltage on E2, the sheath retains curvature at the edge of the wafer with electric field vectors oriented toward smaller radii. With increasing voltage, the sheath thickness above electrode E2 increases relative to the sheath thickness over the wafer. With the width of electrode E2 being only 2 cm, the extension of the sheath over the FR due to voltage on E2 is fairly localized. The curvature of the sheath at the edge of the wafer and the FR due to E1 and E2 have opposite signs. Though admittedly more complex, to some degree, the sheath thickness at the edge of the wafer is the sum of the sheath widths due to the voltages on E1 and E2. The curvature of the sheath at the edge of the wafer, therefore, decreases with increasing voltage on E2. With sufficiently large voltage on E2, the sheath curvature at the edge of the wafer is inverted resulting in the electric field vectors at the edge of the wafer pointing outward to larger radii. The sheath widths over the wafer having radii smaller than 14.5 cm are little affected by the auxiliary electrode.

The current from electrode E2 is transmitted to the plasma through the capacitance of the dielectric FR surrounding E2. Current from E2 is also coupled as displacement current through the FR to electrode E1. From a DC bias perspective, the effective blocking capacitance for E2 is the series capacitance of the discrete blocking capacitor and the capacitance of the dielectric directly above E2 through which the majority of current flowing to the plasma passes. The discrete blocking capacitor is 100 nF, whereas the dielectric directly above E2 has a capacitance of 0.6 nF. The result is that a majority of the time averaged DC bias for E2 appears across the capacitance of the dielectric of the FR and not across the discrete blocking capacitor. For example, for E2 voltage amplitudes of 600 to 5400 V, the voltage on the discrete blocking capacitor is only −170 to −95 V. At the peak of the cathodic cycle, the voltage drop across the dielectric above E2 is 400–700 V.

IEADs incident onto the edge of the wafer (W5) for voltages applied to electrode E2 of 0–5400 V at 5 MHz are shown in Fig. 6. The voltage applied to electrode E1 has a constant amplitude of 1200 V at 5 MHz. The voltages in E1 and E2 are in phase. The angle averaged ion energy distributions (IEDs) and energy averaged ion angular distributions (IADs) for the IEADs in Fig. 6 are in Fig. 7. The IEAD at the edge of the wafer (W5) has a positive tilt of 10° (pointing toward the center of the wafer) without voltage on E2. With increasing voltage on E2, the expanding sheath above the FR progressively straightens the curvature in the sheath at the edge

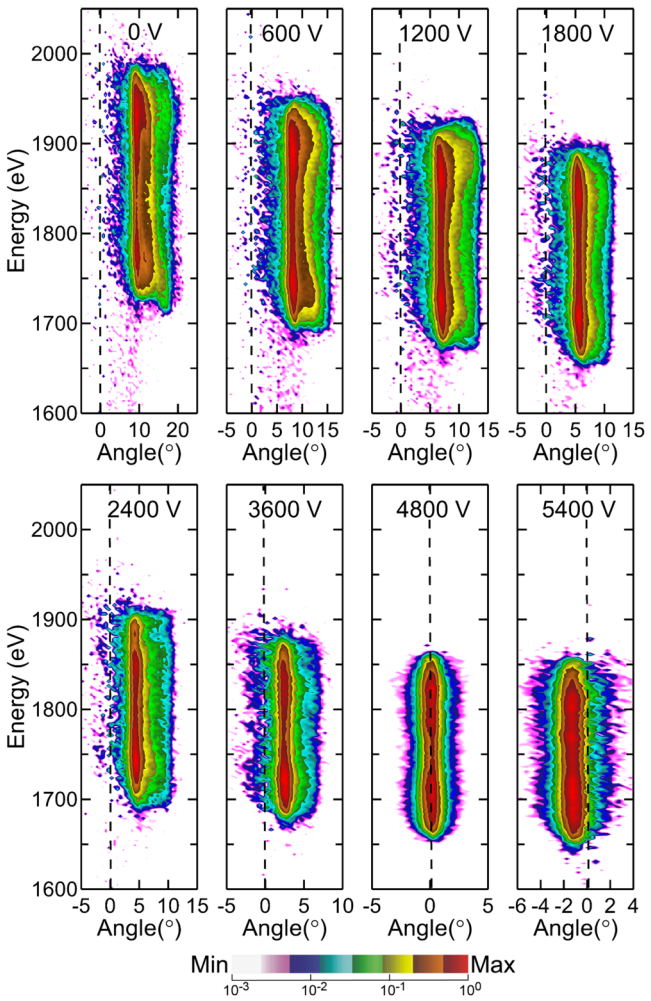

FIG. 6. IEADs incident onto the edge of the wafer (W5) for voltage amplitudes on electrode E2 of 0–5400 V. Images are plotted on a three-decade log-scale. The range of angles may differ for each voltage. The dashed line indicates normal incidence. Positive angles indicate ions whose trajectories are pointing toward the center of the wafer. Negative angles are for ions with trajectories pointing radially outward.

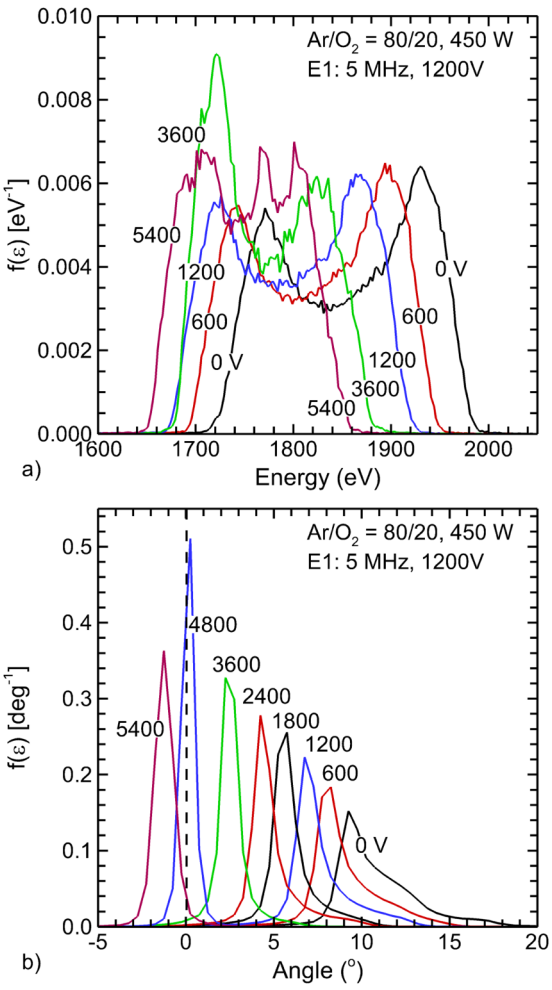

FIG. 7. IEDs and IADs for all ions incident onto the edge of the wafer (W5) for voltages on electrode E2 of 0–5400 V. (a) Angular averaged ion energy distribution (IEDs) and (b) energy averaged angular distributions (IADs). Positive angles are for ions whose trajectories are pointing toward the center of the wafer. Negative angles are for ions with trajectories pointing radially outward.

of the wafer, resulting in a reduction in the tilt of the IEAD incident on the edge of the wafer. With a voltage amplitude of 4800 V on E2, the IEAD on the edge of the wafer has essentially a normal orientation. For voltages on E2 greater than 4800 V, the curvature of the sheath at the edge of the wafer is reversed, which produces electric field vectors pointing outward. The resulting IEAD then has a negative angular tilt, which corresponds to ions striking the edge of the wafer having trajectories pointing radially outward. For a voltage amplitude of 4800 V on E2, the IEADs across the wafer uniformly have normal orientations and essentially the same extent in energy, as shown in Fig. 8.

The average ion energy striking the wafer decreases with increasing voltage on E2. With the voltage amplitude on E1 remaining constant at 1200 V, the decrease in ion energy results from a decrease in the amplitude of the DC bias (less negative), V_{DC}, directly connected to E1. V_{DC} for E1 decreases (less negative with a smaller amplitude) from −1050 V without voltage on E2 to −895 V with 5400 V on E2. This decrease in V_{DC} results from the proximity of E2 and from current sharing to the ground plane. In the absence of E2, current from E1 not passing through the wafer will pass through the FR as displacement current before reaching ground or passing into the plasma. In the absence of E2, the impedance through the FR is large, thereby limiting current. The response of the system is to produce a larger (more negative) V_{DC}. With voltage on E2 (and a current path through E2), the impedance of the FR appears smaller to E1, which is then manifested in a smaller (less negative) V_{DC}.

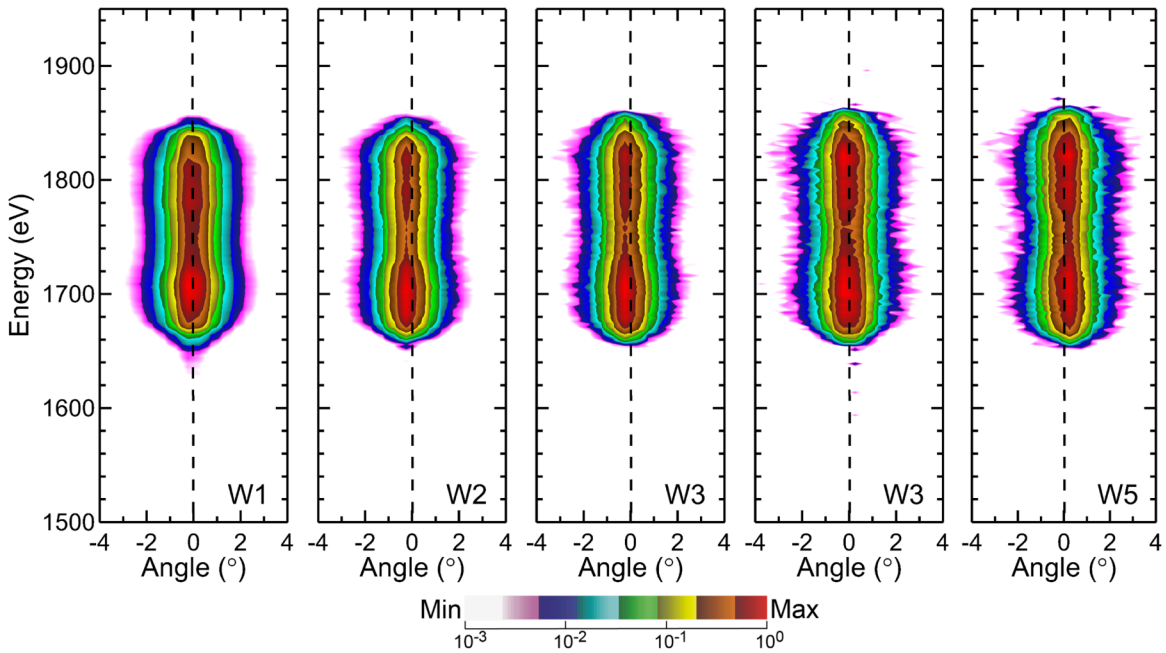

FIG. 8. IEADs incident onto the wafer at positions W1–W5 as noted in Fig. 1(b) with a voltage amplitude of 4800 V on electrode E2. Images are plotted on a three-decade log-scale. The dashed line indicates normal incidence. Positive angles indicate ions whose trajectories are pointing toward the center of the wafer. Negative angles are for ions with trajectories pointing radially outward.

With the sheath curvature at the edge of the wafer resulting, to first order, from the sum of contributions from E1 and E2, sheath curvature will be sensitive to the proximity of the auxiliary electrode E2 to the primary electrode E1. The electron density and electric field vectors for voltage on E2 of 1200 V are shown in Fig. 9 at the peak of the cathodic cycle. The auxiliary electrode E2 is displaced from the primary electrode E1 by 0.5 and 3 cm. The IADs for displacements of 0.5 to 3 cm and IEADs to edge of the wafer (W5) for displacements of 0.5, 1, and 3 cm are shown in Fig. 10. The parameters

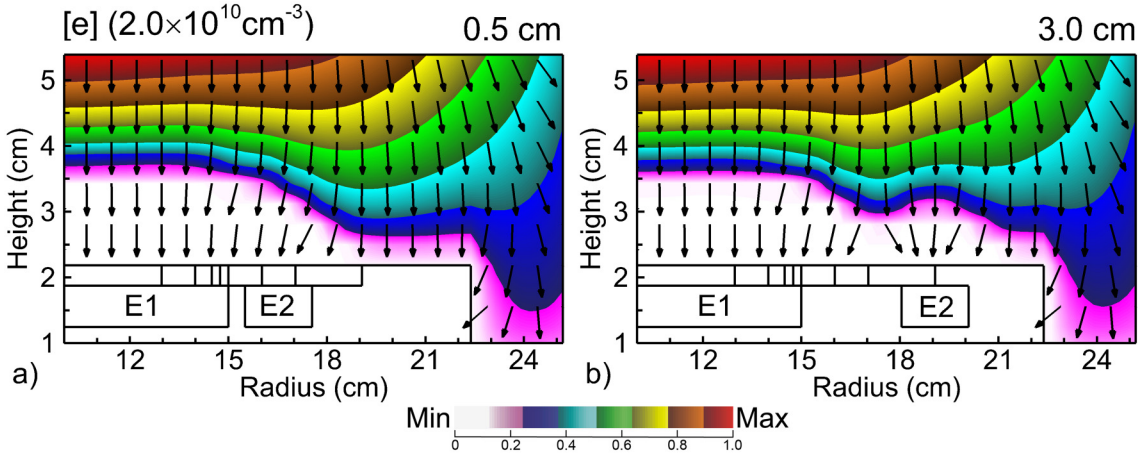

FIG. 9. Electron density and electric field vectors over the wafer edge and the focus ring for a voltage applied to electrode E2 of 1200 V for different displacements d of E2 from the primary electrode. (a) d = 0.5 cm and (b) d = 3 cm. The electron density has a maximum value at the top of the image. Vectors only show the direction of the electric field. The vertical scale in the images is expanded by a factor of 2 for clarity.

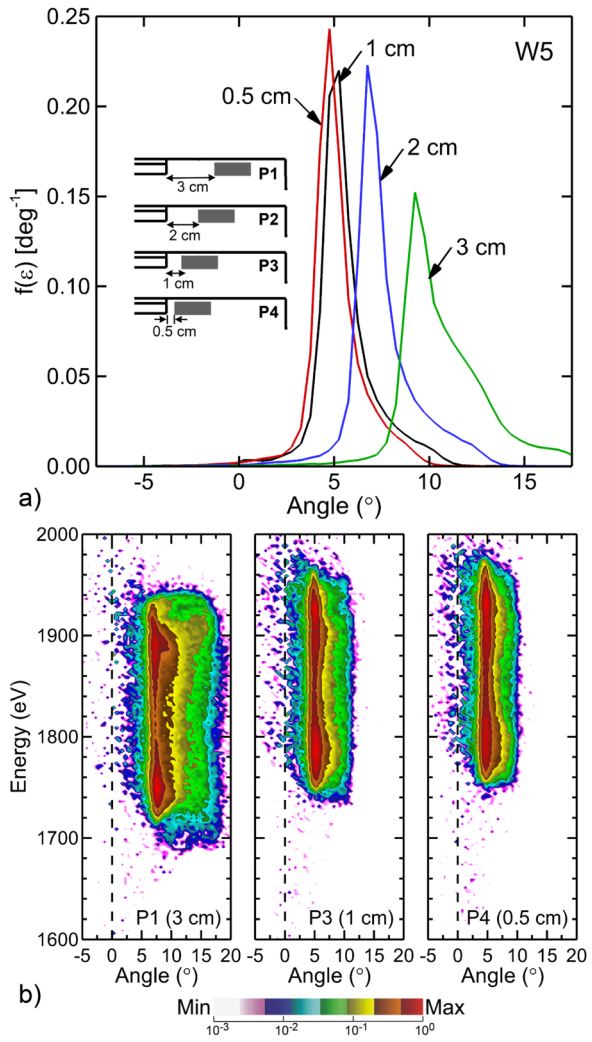

FIG. 10. Properties of ions incident onto the edge of the wafer (W5) for different displacements d of the auxiliary electrode E2 from electrode E1. The RF voltage on E2 is 1200 V amplitude. (a) Ion angular distribution (IAD) for displacement d of E2 of 0.5–3 cm. (b) IEAD for displacements of d = 0.5, 1, and 3 cm. Images are plotted on a three-decade log-scale. The dashed line indicates normal incidence. Positive angles indicate ions whose trajectories are pointing toward the center of the wafer.

for the base case with a displacement of 2 cm are shown in Figs. 6 and 7.

With E2 displaced by 3 cm, the sheath above E2 broadens the curvature of the sheath at the edge of the wafer. Ions originating from over the FR that might have otherwise been incident onto the FR are instead directed onto the edge of the wafer. The IAD (and IEAD) is then tilted to a greater degree than the base case with a displacement of 2 cm. As the displacement between E1 and E2 decreases, the sheaths above electrodes E1 and E2 begin to merge. This merging has the effect of extending the parallel portion of the sheath beyond the edge of the wafer. As a result, the IEAD (and IAD) has a smaller angular tilt. V_{DC} on E1 decreases (less negative) as the displacement of electrode E2 from E1 increases, which results from E1 collecting more current. As E2 is more distance from E1, displacement current from E1 flowing through the focus ring is better able to reach the top of the FR and connect to conduction current in the plasma.

IV. CONCLUDING REMARKS

Results from a computational investigation of the use of an auxiliary ring electrode embedded in the focus ring in a plasma etching reactor were discussed with the goal of controlling the angular tilt of ions incident onto the edge of the wafer. The test system was an inductively coupled plasma sustained in 10 mTorr of an $Ar/O_2 = 80/20$ mixture with 450 W source power. An RF bias was applied to the substrate with a voltage amplitude of 1200 V and a frequency of 5 MHz. The 30 cm diameter primary electrode (E1) was covered by a silicon wafer and surrounded by a dielectric focus ring (FR). For the base case, the trajectories of ions incident onto the wafer were tilted from the normal over the outer several mm of the wafer. This tilt to the IEADs resulted from thinning of the sheath over the FR compared to the sheath over the wafer, which then produced curvature of the sheath at the outer edge of the wafer.

With the RF voltage applied to an auxiliary ring electrode (E2) embedded in the FR, the trajectories of ions could be restored to being normal to the wafer across the entire wafer. This was accomplished by the voltage applied to E2 thickening the sheath over the FR extending to the edge of the wafer. Sheath curvature at the edge of the wafer was reduced, which, in turn, reduced the tilt of ion trajectories onto the edge of the wafer. With sufficient voltage applied to E2 and optimum proximity of E2 to the primary electrode E1, ion trajectories could be made uniform across the entire wafer.

The key to maintaining uniform and normal ion trajectories across and to the edge of the wafer is to maintain a sheath edge that is parallel to the wafer—that is, minimize sheath curvature. Perhaps the ideal way to maintain this lack of sheath curvature is to minimize discontinuities at the edge of the wafer. This could be accomplished by extending the biased electrode beyond the diameter of the wafer. The electrode at larger radii would be covered by a waferlike material having the same electrical properties (permittivity and conductivity) as the wafer. This approach comes with the cost of increasing bias power deposition by the biased electrode by the square of the ratio of the electrode diameter to the wafer diameter. This technique would also introduce a material that would likely be a consumable having a short replacement time.

Another strategy would be to extend the diameter of the biased electrode into the FR, akin to having the auxiliary electrode E2 being placed close to the primary biased electrode E1. Although mechanically straightforward, there would still be sheath thinning above the focus ring. The capacitance of the FR above the extended bias electrode would likely be smaller, and impedance larger, than that of the wafer. As a result, there would be more voltage dropped across the FR compared to the wafer, which would then leave less

voltage for the sheath above the FR. This would produce a thinner sheath over the FR and curvature of the sheath at the edge of the wafer. To minimize this effect, the thickness of the FR above the extended bias electrode should be chosen so that its capacitance is the same as the wafer. This might be accomplished by having a thicker bias electrode beyond the edge of the wafer, which would then thin the FR.

With the impedance of the FR being larger than the wafer, there will be a voltage drop across the FR at the expense of the voltage drop across the sheath. The smaller voltage drop across the sheath over the FR produces thinning of the sheath and sheath curvature at the edge of the wafer. It is for this reason that larger voltages must be applied to the auxiliary electrode E2 to straighten ion trajectories. The larger voltage is needed in order to sufficiently thicken the sheath above the FR to remediate sheath curvature. Some portion of the voltage applied to E2 is dropped across the capacitance of the FR, and so a larger voltage must be applied to E2 compared to E1 so that a similar voltage is dropped across the sheath above the FR.

Just as there is a cost to extending the primary electrode beyond the edge of the wafer, there is also a cost to adding the auxiliary electrode E2. Large voltages on E2 produce high ion energies incident onto the FR, which will increase its rate of erosion, which brings with it the costs to periodically replace the FR. With a higher voltage applied to E2, there must be either a second power supply and matchbox, or transformer circuitry added to the electronics for electrode E1 to provide the higher voltage. In either case, there is additional power dissipated by E2. For example, for the case in which the IEADs were made normal across the edge of the wafer (see Fig. 8), the voltage amplitude on E2 was 4800 V and the voltage applied to E1 was 1200 V. For these conditions, the power deposition by E1 and E2 was nearly equal—about 550 W each. Although we did not fully optimize our geometry, the results of this investigation suggest strategies to lower the voltage and power applied to E2 that are needed to produce a flat sheath across the edge of the wafer. Locating E2 closer to E1 and having a thicker E2 electrode (producing a thinner FR above E2) would both reduce the voltage on E2 required to produce a flat sheath and reduce the power dissipation by E2. Lowering the voltage on E2 also brings the benefit of less erosion of the FR.

This investigation was performed for an ICP with a biased substrate. In ICPs of this sort, ionization is dominantly produced by the antenna delivered power. As a result, the consequences of the auxiliary electrode on IEADs can be isolated from changes in plasma properties that might occur due to ionization by the auxiliary electrode. In capacitively coupled plasmas (CCPs), ionization sources and control of the IEAD are more closely coupled. In dual-frequency CCPs having a high frequency source (many tens of MHz to 100 MHz) and a low frequency bias (less than a few MHz), ionization is dominated by the source and control of the IEAD is dominated by the bias.[34] We expect that the conclusions of this study will apply to CCPs of this type. At the other extreme, single frequency CCP ionization and control of the IEAD come from the same power source. As a result, implementing the recommendations of this study in single frequency CCPs will likely be more challenging.

ACKNOWLEDGMENTS

This work was supported by the U.S. Department of Energy Office of Fusion Energy Sciences (No. DE-SC0024545), the National Science Foundation (No. PHY-2009219), Samsung Electronics, and Lam Research Corp.

AUTHOR DECLARATIONS

Conflict of Interest

The authors have no conflicts to disclose.

Author Contributions

Tugba Piskin: Conceptualization (equal); Formal analysis (lead); Investigation (lead); Methodology (lead); Software (equal); Visualization (lead); Writing – original draft (lead); Writing – review & editing (equal). **Saravanapriyan Sriraman:** Conceptualization (equal); Investigation (supporting); Methodology (supporting); Resources (equal); Supervision (supporting); Writing – review & editing (supporting). **Hyunjae Lee:** Investigation (supporting); Methodology (supporting); Resources (equal); Supervision (supporting); Writing – review & editing (supporting). **Sang Ki Nam:** Investigation (supporting); Methodology (supporting); Resources (equal); Supervision (supporting); Writing – review & editing (supporting). **Mark J. Kushner:** Formal analysis (equal); Funding acquisition (equal); Investigation (equal); Methodology (equal); Project administration (equal); Software (equal); Supervision (equal); Visualization (equal); Writing – review & editing (equal).

DATA AVAILABILITY

The data that support the findings of this study are available within the article and are available from the corresponding author upon reasonable request.

REFERENCES

[1]C. G. N. Lee, K. J. Kanarik, and R. A. Gottscho, J. Phys. D: Appl. Phys. **47**, 273001 (2014).
[2]V. M. Donnelly and A. Kornbilt, J. Vac. Sci. Technol. A **31**, 050825 (2013).
[3]I. Adamovich *et al.*, J. Phys. D: Appl. Phys. **50**, 323001 (2017).
[4]D. Kim and D. J. Economou, J. Appl. Phys. **94**, 2852 (2003).
[5]M. Y. Yoon, H. J. Yeom, J. H. Kim, J. R. Jeong, and H. C. Lee, Appl. Surf. Sci. **595**, 153462 (2022).
[6]S. Huang, C. Huard, S. Shim, S. K. Nam, I. C. Song, S. Lu, and M. J. Kushner, J. Vac. Sci. Technol. A **37**, 031304 (2019).
[7]R. J. Belen, S. Gomez, M. Kiehlbauch, and E. S. Aydil, J. Vac. Sci. Technol. A **24**, 2176 (2006).
[8]M. Kubota and T. Shima, U.S. patent 2015/0243488 A1 (27 August 2016).
[9]T. Yagisawa, T. Shimada, and T. Makabe, J. Vac. Sci. Technol. B **23**, 2212 (2005).
[10]L. Tong, Jpn. J. Appl. Phys. **54**, 06GA01 (2015).
[11]Y. Xiao, Y. Du, C. Smith, S. K. Nam, H. Lee, J. Y. Lee, and S. Shannon, J. Vac. Sci. Technol. A **39**, 043006 (2021).
[12]Y. Qian, W. Gekelman, P. Pribyl, T. Piskin, and A. Paterson, Phys. Plasmas **31**, 063507 (2024).
[13]Y. Zhang, M. J. Kushner, S. Sriraman, A. Marakhtanov, J. Holland, and A. Paterson, J. Vac. Sci. Technol. A **33**, 031302 (2015).
[14]X. Wang, H. Lee, S. K. Nam, and M. J. Kushner, J. Vac. Sci. Technol. A **39**, 063002 (2021).

[15]J. S. Kim, M. Y. Hur, H. J. Kim, and H. J. Lee, J. Appl. Phys. **126**, 233301 (2019).
[16]N. Y. Babaeva and M. J. Kushner, J. Phys. D: Appl. Phys. **41**, 062004 (2008).
[17]F. F. Ma, Q. Z. Zhang, D. M. Han, Z. L. Xiong, M. Gao, and Y. N. Wang, J. Vac. Sci. Technol. A **41**, 053002 (2023).
[18]D. Kim, D. J. Economou, J. R. Woodworth, P. A. Miller, R. J. Shul, B. P. Aragon, T. W. Hamilton, and C. G. Willison, IEEE Trans. Plasma Sci. **31**, 691 (2003).
[19]Y. Zhang, S. Sriraman, and A. Paterson, U.S. patent 20190362940A1 (28 November 2019).
[20]D. Kim and D. J. Economou, IEEE Trans. Plasma Sci. **30**, 2048 (2002).
[21]C. C. Huang, U.S. patent US6767844B2 (3 July 2002).
[22]W. Johnson, U.S. patent 10/378,992 (5 March 2003).
[23]Y. Xiao, J. Brandon, J. Morsell, S. K. Nam, K. Bae, J. Y. Lee, and S. Shannon, J. Vac. Sci. Technol. A **41**, 033008 (2023).
[24]S. Sriraman, T. A. Kamp, and A. Paterson, U.S. patent US010163610B2 (25 December 2018).
[25]M. J. Kushner, J. Phys. D: Appl. Phys. **42**, 194013 (2009).
[26]F. Krüger, H. Lee, S. K. Nam, and M. J. Kushner, J. Vac. Sci. Technol. A **41**, 013006 (2023).
[27]E. Litch, H. Lee, S. K. Nam, and M. J. Kushner, J. Vac. Sci. Technol. A **43**, 033001 (2025).
[28]T. Piskin, Y. Qian, P. Pribyl, W. Gekelman, and M. J. Kushner, J. Appl. Phys. **133**, 173302 (2023).
[29]C. Qu, S. J. Lanham, S. C. Shannon, S. K. Nam, and M. J. Kushner, J. Appl. Phys. **127**, 133302 (2020).
[30]S. Huang, V. Volynets, J. R. Hamilton, S. Lee, I.-C. Song, S. Lu, J. Tennyson, and M. J. Kushner, J. Vac. Sci. Technol. A **35**, 031302 (2017).
[31]T. Panagopoulos and D. J. Economou, J. Appl. Phys. **85**, 3435 (1999).
[32]M. A. Lieberman and A. J. Lichtenberg, *Principles of Plasma Discharges and Materials Processing* (Wiley, New York, 1994).
[33]Z. L. Dai and Y. N. Wang, Phys. Rev. E **69**, 036403 (2004).
[34]S. Rauf, P. Tian, J. Kenney, and L. Dorf, J. Vac. Sci. Technol. B **40**, 032202 (2022).